Osteoblast connexin43 modulates skeletal architecture by regulating both arms of bone remodeling

Marcus Watkins[a], Susan K. Grimston[a], Jin Yi Norris[a], Bertrand Guillotin[a], Angela Shaw[a], Elia Beniash[b], and Roberto Civitelli[a]

[a]Division of Bone and Mineral Diseases, Departments of Internal Medicine and Cell Biology and Physiology, Washington University School of Medicine, St. Louis, MO 63110; [b]School of Dental Medicine Center for Craniofacial Regeneration, McGowan Institute for Regenerative Medicine Bioengineering, University of Pittsburgh, Pittsburgh, PA 15260

ABSTRACT **Connexin43 (Cx43) has an important role in skeletal homeostasis, and Cx43 gene (*Gja1*) mutations have been linked to oculodentodigital dysplasia (ODDD), a human disorder characterized by prominent skeletal abnormalities. To determine the function of Cx43 at early steps of osteogenesis and its role in the ODDD skeletal phenotype, we have used the *Dermo1* promoter to drive *Gja1* ablation or induce an ODDD mutation in the chondro-osteogenic linage. Both *Gja1* null and ODDD mutant mice develop age-related osteopenia, primarily due to a progressive enlargement of the medullary cavity and cortical thinning. This phenotype is the consequence of a high bone turnover state, with increased endocortical osteoclast-mediated bone resorption and increased periosteal bone apposition. Increased bone resorption is a noncell autonomous defect, caused by exuberant stimulation of osteoclastogenesis by Cx43-deficient bone marrow stromal cells, via decreased *Opg* production. The latter is part of a broad defect in osteoblast differentiation and function, which also results in abnormal structural and material properties of bone leading to decreased resistance to mechanical load. Thus Cx43 in osteogenic cells is a critical regulator of both arms of the bone remodeling cycle, its absence causing structural changes remindful of aged or disused bone.**

Monitoring Editor
Richard K Assoian
University of Pennsylvania

Received: Jul 7, 2010
Revised: Dec 28, 2010
Accepted: Feb 15, 2011

INTRODUCTION

After embryonic development, the skeleton undergoes continuous remodeling during adult life to ensure biomechanical integrity, rejuvenate aging bone, and repair injuries. Bone remodeling is orchestrated by bone-resorbing cells—osteoclasts—and bone-forming cells—osteoblasts—as well as osteocytes, which are embedded into the mineralized tissue. In addition to endocrine, paracrine, and autocrine factors, direct cell–cell communication via gap junctions is an important mechanism by which bone cells coordinate their activities. Abundant gap junctions are present between osteocytic processes, between osteocytes and osteoblasts on the bone surface, and among osteoblasts (Doty, 1981; Palumbo *et al.*, 1990). Gap junctions are arrays of hexameric transmembrane channels, called connexons, formed by protein subunits called connexins. When two connexons are in register on opposing cells, an aqueous conduit is formed between two cells—a gap junction channel—which allows cell-to-cell diffusion of ions, metabolites, and small signaling molecules (Goodenough *et al.*, 1996). Connexons can also exist as individual channels, not paired with apposing connexons, thus functioning as large transmembrane channels (Goodenough and Paul, 2003).

At least three connexins are present in bone cells, each providing unique permeability, ion selectivity, and electric conductance.

This article was published online ahead of print in MBoC in Press (http://www.molbiolcell.org/cgi/doi/10.1091/mbc.E10-07-0571) on February 23, 2011.

Roberto Civitelli has a Material Transfer Agreement with Zealand Pharma, Glostrup, Denmark, for the use of gap junction modifying peptides, but receives no honoraria or research funds from Zealand. None of the other authors have financial conflicts of interest.

Address correspondence to: Marcus Watkins (mwatkins@dom.wustl.edu).

Abbreviations used: β-gal, β-galactosidase; cODDD, conditional oculodentodigital dysplasia (*DM1;Gja1*$^{+/fl(G138R)}$); cKO, *Gja1* conditional knockout (*DM1;Cx43*$^{-/fl}$); Cx43, connexin43; DM1-Cre, *Dermo1* promoter driven Cre recombinase; ODDD, oculodentodigital dysplasia; WTfl, wild-type comparison for *Gja1* conditional knockout (*Cx43*$^{wt/fl}$); WTod, wild-type comparison for conditional oculodentodigital dysplasia.

Connexin43 (Cx43) is the most abundant, and multiple lines of evidence have established an important role for Cx43 in skeletal development and for the function and survival of osteoblasts and osteocytes (see Stains and Civitelli, 2005; Civitelli *et al.*, 2008, for review). In particular, germline ablation of *Gja1*, the gene encoding for Cx43, results in delayed endochondral and intramembranous ossification, osteoblast dysfunction, and craniofacial abnormalities (Lecanda *et al.*, 2000). Because of the perinatal lethality of the germline mutation, tissue-specific *Gja1* ablation models have been developed. We have previously reported that conditional *Gja1* ablation driven by a fragment of the *Col1A1* promoter, which expresses in committed osteoblasts, results in accrual of a low peak bone mass and an attenuated response to the anabolic effects of parathyroid hormone, the consequence of an osteoblast defect (Chung *et al.*, 2006). In subsequent studies, we have also shown that these mice have enlarged diaphyses and thin cortices of the long bones, decreased bone strength, as well as an attenuated anabolic response to mechanical load (Grimston *et al.*, 2006, 2008). On the other hand, others have reported that *Gja1* ablation in more mature osteoblasts and osteocytes using the *Bgalp* promoter causes no abnormalities in bone mass and does not prevent glucocorticoid-induced bone loss. However, it precludes the effect of bisphosphonates on apoptosis (Plotkin *et al.*, 2008), decreases cortical bone strength, and causes structural abnormalities similar to *Gja1* deletion in less mature osteoblasts (Bivi *et al.*, 2009).

Further proof of the critical role of Cx43 in skeletal biology is provided by the identification of *Gja1* mutations as the cause of the autosomal dominant disorder oculodentodigital dysplasia (ODDD), characterized by multi-organ but primarily skeletal abnormalities, with syndactyly of the hands, craniofacial dysmorphisms with cranial hyperostosis, and broad tubular bones (Loddenkemper *et al.*, 2002; Paznekas *et al.*, 2003; Kjaer *et al.*, 2004). Two *Gja1* mouse mutants have been described with skeletal phenotypes closely resembling the human disease, including syndactyly and craniofacial malformations (Flenniken *et al.*, 2005; Dobrowolski *et al.*, 2008). These animal models have also disclosed additional aspects of ODDD that are unknown or unreported in humans, in particular generalized osteopenia and cortical thinning, which could heavily impact on fracture risk and morbidity in ODDD patients.

Despite significant progress on Cx43 skeletal biology, a number of key questions remain unanswered. Accumulated in vivo data suggest that Cx43 may be important at early steps of osteogenesis, perhaps at the time of osteogenic commitment from undifferentiated precursors. Lack of reliable strategies to induce selective gene ablation in osteogenic precursors has so far precluded testing this hypothesis in vivo. Although osteogenic lineage defects are evident in Cx43-deficient mice, these defects alone cannot explain all the phenotypic features produced by *Gja1* ablation in differentiated osteoblasts, specifically, the widened diaphyses of long bones (Grimston *et al.*, 2008) and lack of sensitivity to skeletal mechanical unloading (Grimston, Goldberg, Watkins, Brodt, Silva, and Civitelli, unpublished data), both of which point to a bone resorption abnormality. Aside from in vitro studies suggesting a role of Cx43 in osteoclast function (Ransjo *et al.*, 2003; Matemba *et al.*, 2006), bone resorption has not been analyzed in Cx43-deficient animals. Furthermore, although ODDD mutations are loss-of-function and dominant negative for wild-type Cx43 (Roscoe *et al.*, 2005; Gong *et al.*, 2007), germline or conditional *Gja1* ablation in bone-forming cells does not exactly phenocopy ODDD, lacking primarily the craniofacial malformations. This implies a more complex pathobiology of Cx43 mutations in the cranium relative to the axial and appendicular skeleton. Finally, introduction of ODDD mutants in osteoblasts in vitro alters only expression of late differentiation genes (McLachlan *et al.*, 2008). These abnormalities are insufficient to explain the whole ODDD phenotype, raising the possibility that the ODDD mutants may interfere with normal Cx43 function at earlier phases of osteoblast differentiation or via other mechanisms.

In this study, we have used the *Dermo1/Twist2* (*DM1*) promoter to drive Cre expression (DM1-Cre) and obtain an early but selective *Gja1* ablation in the chondro-osteogenic lineage (Yu *et al.*, 2003). We have also used DM1-Cre mice to induce an ODDD mutation selectively in chondro-osteogenic cells. *Dermo1/Twist2* is expressed at E9.5 in mesodermal tissues (Li *et al.*, 1995), and during endocrondral ossification is present in condensed mesenchyme from which chondrocytes and osteoblasts are derived (Yu *et al.*, 2003). This genetic approach allows examination of the role of Cx43 at early stages of osteogenic cell differentiation starting at an early embryologic stage, up to skeletal adulthood.

RESULTS

DM1;Cre-mediated *Gja1* deletion in bone cells

As postnatal *Dermo1/Twist2* expression has not been fully characterized, we first assessed gene recombination in *DM1;Gja1*$^{-/fl}$ (cKO) adult animals. Cx43 immunoreactive bands were barely detectable in cKO whole-bone protein extracts of 1-mo-old mice, whereas they were intense in the *Gja1*$^{fl/wt}$ (WTfl) extracts (Figure 1A). Conversely, bands corresponding to β-galactosidase (β-gal) were detected only in cKO but not in WTfl extract (Figure 1A), consistent with effective *LacZ*/*Gja1* gene replacement in mutant mice. *Gja1* deletion was also confirmed by positive β-gal staining of tibia sections from 1-mo-old mice. Whereas no staining was observed in sections from WTfl littermates (Figure 1B, a′–c′), in cKO sections, specific β-gal staining was observed in cells lining the endocortical surface and in the periosteum, in cells slightly away from the endosteal bone surface, and in osteocytes (Figure 1Bd′). However, very little if any β-gal staining was observed in cells on trabecular surfaces or in trabecular osteocytes (Figure 1Be′), and no staining was present in growth plate chondrocytes (Figure 1Bf′). Because *DM1-Cre* activity had been reported in both the growth plate and trabecular bone (Yu *et al.*, 2003), we mated *DM1-Cre* mice with *ROSA26* mice to determine the field of postnatal *DM1-Cre* expression. Clear β-gal staining was observed in cortical osteoblast and osteocytes (Figure 1Bg′) but also in trabecular osteoblasts (Figure 1Bh′) as well as growth plate chondrocytes (Figure 1Bi′), suggesting that lack of β-gal-positive cells in trabecular bone and growth plates of cKO mice most likely represents very low levels of *Gja1* expression, rather than lack of Cre activity. Importantly, *LacZ* activity persisted in cortical bone at least up to 6 mo of age but disappeared by 12 mo (Supplemental Figure S1). Long-term persistence of recombined cells may reflect postnatal expression of *DM1* or a long life cycle of the originally recombined chondro-osteogenic precursor cells and their progeny. Thus *DM1-Cre* mice represent a good model of selective gene inactivation in the chondro-osteogenic lineage during the first 6 mo of postnatal life.

Delayed mineralization and low bone mass in cKO and cODDD mice

All genotypes from both mating schemes were obtained at the expected Mendelian frequency and all were viable. Whole-mount alizarin red/alcian blue staining of newborn mice revealed only minor dysmorphisms in cKO (Figure 2A), specifically a hypoplastic skull with smaller parietal and interparietal bones and smaller mandible. There was also a modest reduction in chest cavity due to short ribs and slightly shorter tibias and femurs. Newborn *DM1;Gja1*$^{+/fl(G138R)}$

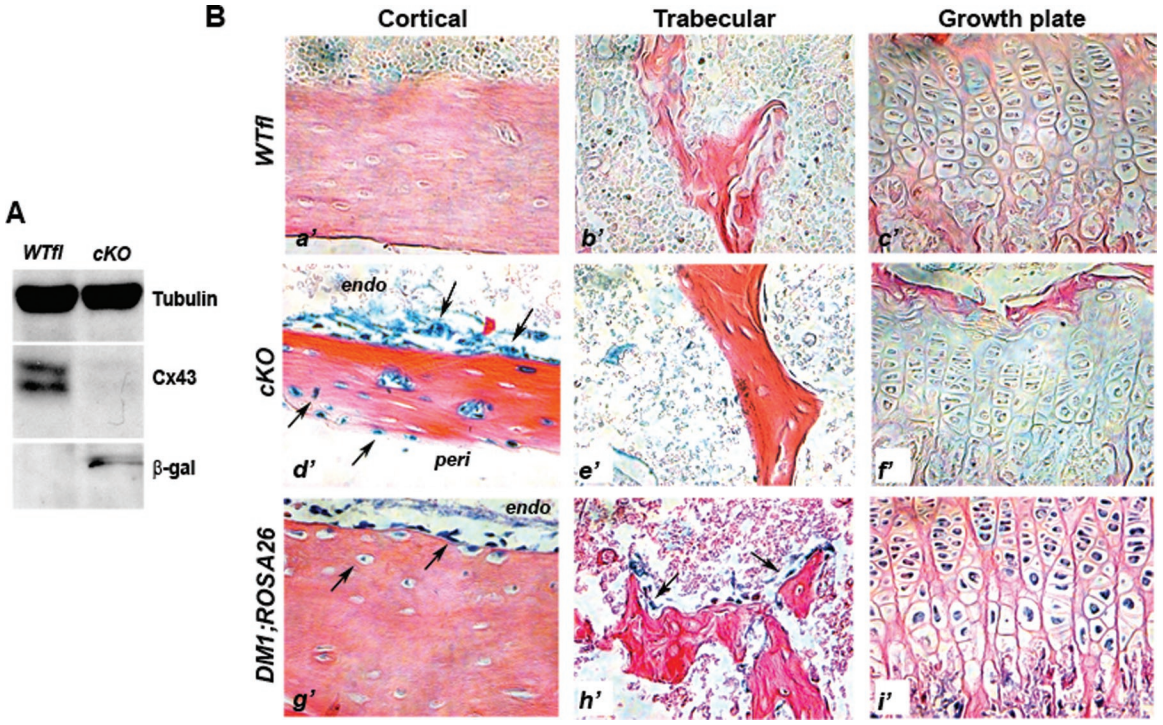

FIGURE 1: Cre-mediated replacement of *Gja1*. (A) Western blot analysis of whole-bone protein extracts from 3-mo-old mice showing strong expression of Cx43 in WTfl extracts and barely detectable immunoreactivity in cKO extracts. *LacZ/Gja1* gene replacement was confirmed by the presence of β-gal immunoreactive bands only in cKO protein extracts. (B) β-gal-stained tibia sections of 1-mo-old mice showing specific β-gal staining present in the cKO but not the WTfl tibia sections. In the cKO bones, specific β-gal staining was observed in cells lining the endocortical surface, the periosteum, and in osteocytes (d'–arrows); however, very little β-gal staining was present in the trabeculae (e'), and none in the growth plate chondrocytes (f'). Comparative sections from 1-mo-old *DM1;ROSA26* mice showing β-gal staining in cells lining the endocortical surface and osteocytes (g'), trabecular osteoblasts (h'), and growth plate chondrocytes (i').

(cODDD) mice exhibited only skull hypomineralization, without the dysmorphic features of cKO mice (Figure 2B). At 1 mo of age, skulls of cKO mice were still significantly hypomineralized, as shown by μCT, with hypoplastic parietal, interparietal, and occipital bones relative to control littermates (Figure 2C), whereas cODDD skulls appeared normally mineralized though slightly smaller than control littermates at this age (Figure 2D).

Whole-body bone mineral density (BMD) monitored by dual-energy x-ray absorptiometry (DXA) up to 1 yr of age revealed that both Cx43 cKO and cODDD mice were significantly osteopenic relative to their respective WT littermates (Figure 2, E and F). This low bone mass phenotype was evident at 1 mo of age and persisted until 10 mo in both cKO and cODDD groups. The largest differences in BMD (~40%) were observed at younger ages, in both mutant groups, with a tendency toward partial recovery after 4 mo of age, and 8–12% difference remaining at 12 mo of age in both groups.

Altered bone structure in *Gja1* mutants

Structural analysis was performed by μCT in femurs of 3-mo-old animals postmortem. Macroscopically, femurs of both cKO (Figure 3A) and cODDD mice (Figure 3G) were ~10% shorter in both mutants, a significant difference in both cases (Figure 3, B and H), and in both cases there was an evident tubulation of the femoral shaft, with larger medullary cavity. However, no differences in bone volume/tissue volume or other trabecular structural parameters were observed in either cKO or cODDD femurs relative to their controls (Supplemental Figure S2). Accordingly, static histomorphometric analysis of cKO bone sections revealed no change in trabecular osteoblast or osteoclast numbers per bone surface (Supplemental Figure S2).

Cross-sectional analysis of the femoral diaphysis confirmed a statistically significant larger total tissue area in both cKO (Figure 3, C and D; Supplemental Figure S3) and cODDD mice (Figure 3, I and J; Supplemental Figure S3). Marrow area was also increased in both mutant mice (Supplemental Figure S3, A and C), though the differences were larger in the cKO than in the cODDD (43 ± 5% vs. 30 ± 6% relative to WT, respectively). Cortical thickness was significantly decreased in both cKO (41 ± 11% of WTfl) and cODDD mice (20 ± 7% of WTod) (Figure 3, E and K). Accordingly, the calculated cross-sectional moment of inertia was significantly increased in the Cx43 cKO compared with WTfl (Supplemental Figure S3, B and D), suggestive of a greater resistance to mechanical strain in the anterior/posterior direction. However, direct assessment of resistance to load, in a three-point bending test to failure, produced rather the opposite results, as ultimate force to failure was lower in cKO compared with WT bones (Supplemental Figure S3E). Although the differences were not significantly different, most cKO bones bent in half without breaking. Because of this unexpected outcome, we also assessed yield force, a point at which further load will cause permanent deformation. This measurement was significantly lower in the cKO compared with WTfl (Figure 3F). Similar trends were obtained with the cODDD bones, although the differences against WTod were not statistically significant (Figure 3L and Supplemental Figure S3F). Unlike the Cx43 cKO bones, all the bones from the cODDD mice did break in the three-point bending test.

Changes in bone formation rates in cKO mice

Because the skeletal phenotypes of cKO and cODDD mice were similar, from this point on we present data for the cKO mice only, as

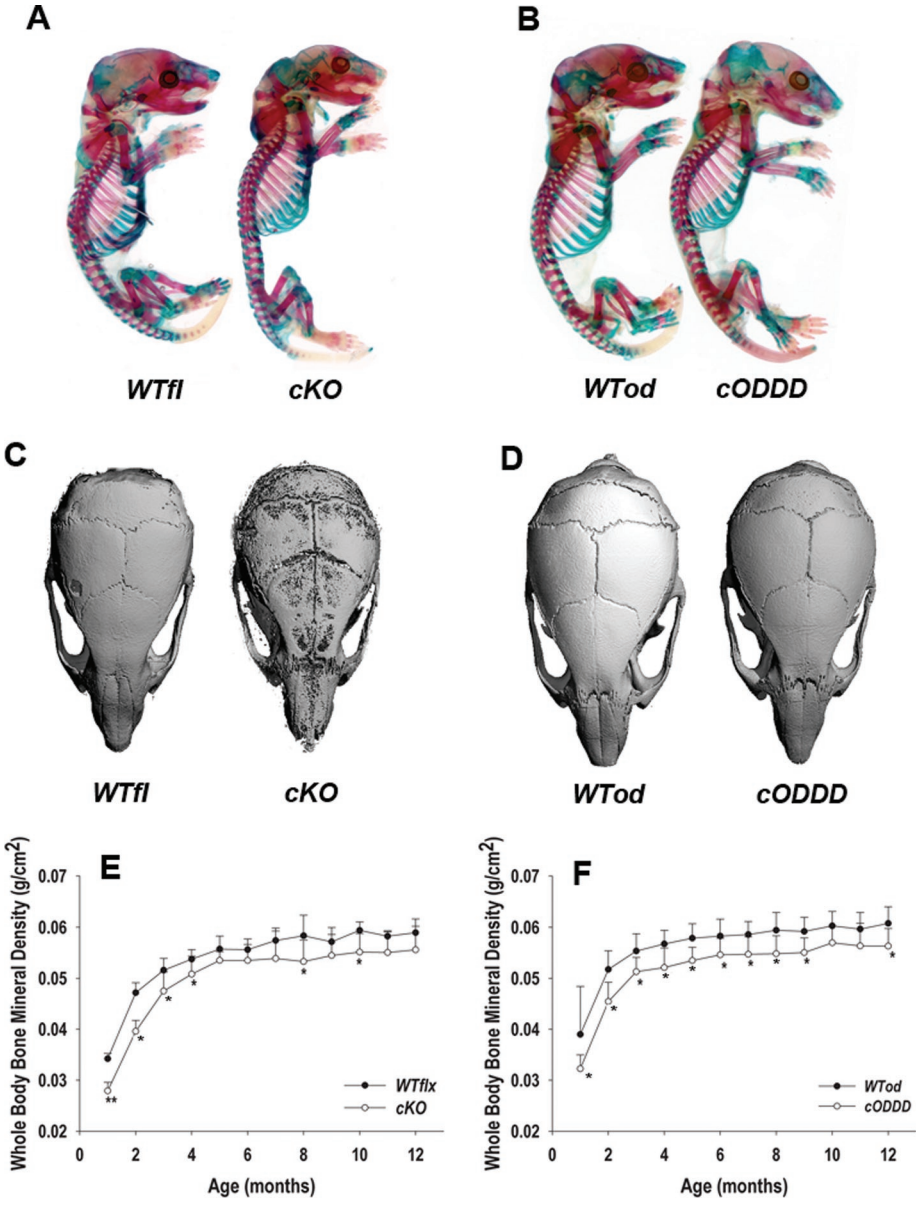

FIGURE 2: Low bone mass and delayed mineralization in cKO and cODDD mice. (A) Alizarin red and alcian blue stained newborn whole mounts showing malformed, hypoplastic cranial vault and smaller thoracic cage in cKO compared with WTfl littermates. (B) Skull hypomineralization but no dysmorphic features are seen in cODDD newborn mice compared with WTod littermates. (C) MicroCT reconstructions of skulls from 1-mo-old cKO mice showing hypoplastic parietal, interparietal, and occipital bones compared with WTfl litermates; but (D) normal mineralization in cODDD skulls compared with WTod. (E) Whole-bone mineral density, monitored by DXA at monthly intervals is significantly lower in cKO and (F) cODDD relative to their comparative WT littermates up to 4 mo of age, with a trend toward partial recovery at later time points (*, $P < 0.05$ for *Gja1* mutants vs. comparative WT, 2-way ANOVA; n = 10).

they exhibit more severe phenotypic changes. Representative fluorescent micrographs of calcein-labeled longitudinal sections of cortical bone show a dramatic difference in the size and distribution of double labels. Whereas in the WTfl, double labels were only seen in the endocortical surface, in the mutant bones, double labels were abundant on the periosteal surface, more than in the endosteum (Figure 4A). Accordingly, dynamic indices of bone formation (BFR/BS and MAR) calculated from the growth plate to mid-diaphysis of the femur were significantly reduced on the endosteal surface of cKO bones, whereas they were strikingly increased on the periosteal surface (Figure 4, B and C). To determine the overall impact of this shift of bone formation from the endosteum to the periosteum, we measured serum osteocalcin levels, a biochemical marker of bone formation. Significantly higher (>40%) serum osteocalcin was detected in Cx43-deficient mice relative to WTfl (Figure 4D), suggesting an exuberant periosteal bone formation in the face of decreased bone formation at the endosteal surface.

Altered cortical bone matrix and hypomineralization in cKO mice

The decreased bone strength of *Gja1* mutant bones, in spite of an increased geometric moment of inertia, implies an abnormality in the material properties of mutant bones. Using a Masson's trichrome stain, we excluded an increased osteoid thickness in cKO bones, thus ruling out osteomalacia as a potential cause of the decreased bone strength (Figure 5A). Interestingly, the cell layer on the periosteal surface was more prominent in cKO than in WTfl sections, consistent with increased osteoblast activity on the periosteum. Low-magnification cross-sections of the femur confirmed the larger size, increased marrow area, and thinner cortex and also revealed increased cortical porosity in the Cx43 cKO bones, with large areas of the cortex undergoing a process of spongiosation (Figure 5B). Analysis of tibial cortical sections under polarized light after picrosirius red staining revealed more disorganized birefringence, especially on the periosteal surface of cKO sections, reflective of disorganized collagen fibers and an appearance of woven bone (Figure 5C). Quantification of the birefringence pattern revealed that fiber orientation in the WTfl bones clustered around 90 degrees, as expected; wheareas in the cKO bone, collagen fiber orientation was highly variable and spread across the whole range (Figure 5D). Further quantification of the degree of disorder of collagen bundles revealed that enthropy was 3.98 ± 0.57 in cKO, compared with 2.90 ± 0.024 in WTfl ($P < 0.05$), respectively, about a 40% difference. On the basis of such abnormalities in collagen fiber organization, we measured the abundance of gene products known to be involved in extracellular collagen processing, using RNA extracted from femurs from which the bone marrow had been removed. Interestingly, lysyl oxidase (*Lox*) mRNA was significantly reduced in Cx43 cKO mice (~57%) compared WTfl mice, whereas procollagen lysyl hydroxylase (*Plod*) and prolyl 3-hydroxylase (*P3HA4*) were unchanged (Figure 5E). By μCT, mineral density in the cKO cortical bone was significantly reduced ($-9 \pm 2\%$) relative to WTfl (Figure 5F). Despite decreased *lox* mRNA, we found no major abnormality in collagen cross-linking in cKO bones but rather a decrease in collagen mRNA abundance (not shown). Fourier transform

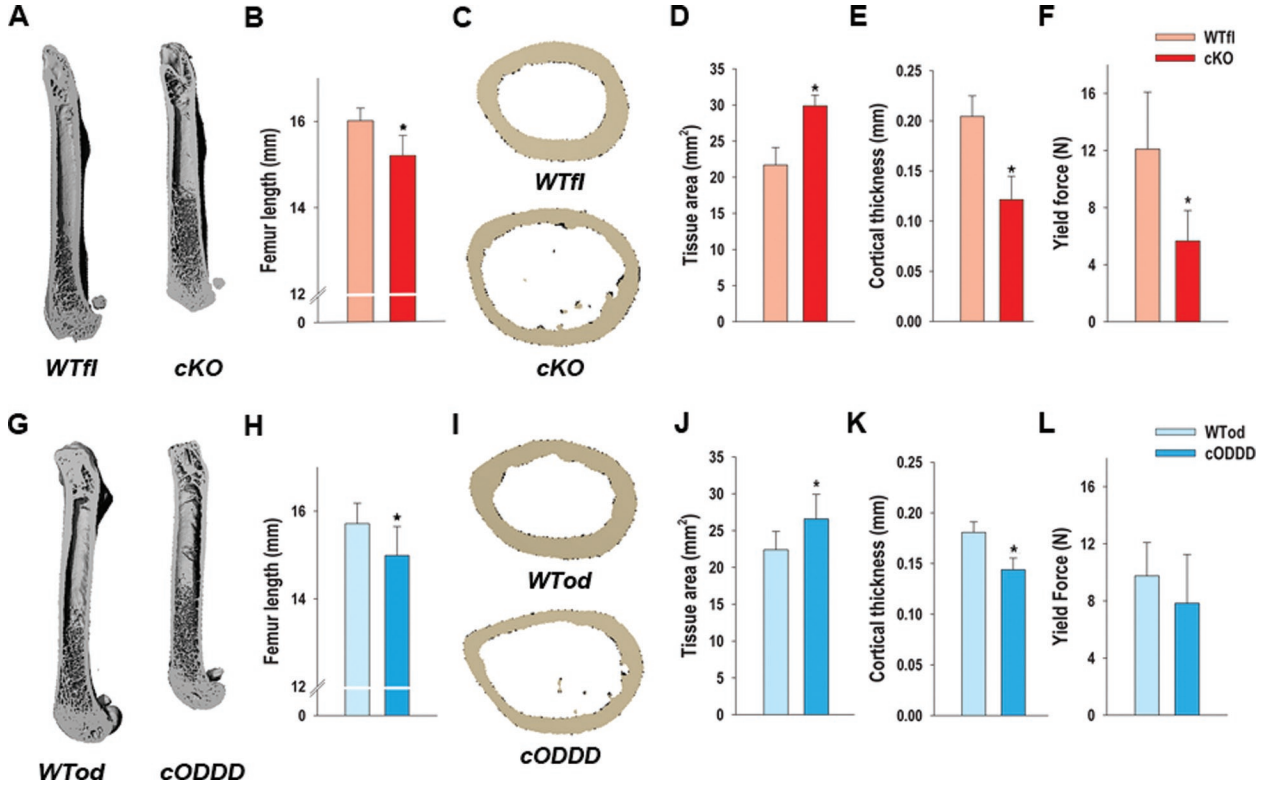

FIGURE 3: Altered bone structure and strength in *Gja1* mutants. (A) MicroCT (μCT) reconstructions of femurs from 1-mo-old WTfl and cKO mice showing shorter, tubular femoral shafts with larger medullary cavities. (B) Femur length is significantly reduced in the cKO relative to their littermate WT controls. (C) Cross-sections of femurs at middisphysis by μCT revealing a wider cortical bone section and marrow cavity of cKO femurs relative to WTfl. (D) Tissue area is significantly higher and (E) cortical thickness is significantly lower in cKO compared with WTfl. (F) Yield force, measured using a three-point bending test, is reduced relative to WTfl. (G) μCT reconstructions of femurs from 1-mo-old WTod and cODDD mice. (H) Femur length is significantly reduced in cODDD mice relative to their littermate WT controls. (I) Cross-sections of femurs at middisphysis by μCT revealing a wider cortical bone section and marrow cavity of cODDD femurs relative to WTod. (J) Tissue area is significantly higher and (K) cortical thickness is significantly lower in cODDD compared with WTod. (L) Yield force is not significantly different in cODDD, compared with WTod (*, $P < 0.05$, vs. WT; *t*-test for unpaired samples, n = 5).

infrared spectroscopy (FTIR) analysis of bone samples from the KO animals suggested that cKO femurs are less mineralized relative to WTfl, and the mineral appeared less mature (Supplemental Figure S4), although these differences were not significant.

Abnormal osteoblast differentiation and function in cKO mice

To investigate the cellular and molecular mechanisms leading to the phenotype of Cx43-deficient mice, we profiled gene expression in cortical bone cells of mutant and wild-type mice using real-time quantitative PCR. Cortical bone extracts (excluding the bone marrow, but including the periosteum) confirmed a greater than 80% decrease in *Gja1* expression (Figure 6A), consistent with *Gja1* recombination in vivo (see Figure 1). There was no difference in *Runx2* mRNA abundance; but other osteoblastic genes, all down-stream of *Runx2*, were down-regulated in cKO bones relative to WTfl, including *Osx* (42%), *Alpl* (31%), and *Col1A1* (41%), although *OPN* and *BSP* mRNA were unaffected (Figure 6A). Furthermore, mRNA abundance for osteocyte genes *Dmp1* and *Sost* was also significantly reduced in cKO (42% and 62%, respectively; Figure 6B). However, the number of osteocytes per cortical surface area was not different between cKO mice and WTfl (Figures 5A and 6C). Because *DM-1* induces *Gja1* ablation early in the chondro-osteogenic lineage, we performed CFU assays to determine whether the number of stromal cell precursors was also affected by *Gja1* deletion. Intriguingly, the number of CFU-fibroblast, an index of stromal uncommitted precursors, was significantly increased in the cKO relative to WTfl bone marrow (Figure 6, D and E). Even more surprisingly, the number of CFU-osteoblast, an index of osteogenic precursors, was also increased in the mutant animals (Figure 6, F and G). Finally, cell proliferation rate was almost fourfold higher in cKO than in WTfl bone marrow stromal cells (Figure 6H).

Increased osteoclastogenesis and bone resorption in cKO mice

Bone marrow cavity expansion, a feature common to both cKO and cODDD mice, implies increased endocortical bone resorption. Consistent with this hypothesis, we found the number of endocortical TRAP+ osteoclasts per bone perimeter to be three- to fourfold higher in cKO bones than in WTfl (Figure 7, A and B). Serum levels of C-terminal telopeptides of type I collagen, a biochemical marker of bone resorption, were significantly higher in cKO than in WTfl mice, confirming that the increased endocortical osteoclast number reflects increased bone resorption (Figure 7C).

Because *Gja1* ablation in this cKO model occurs specifically in cells of the osteoblast lineage, we determined whether the

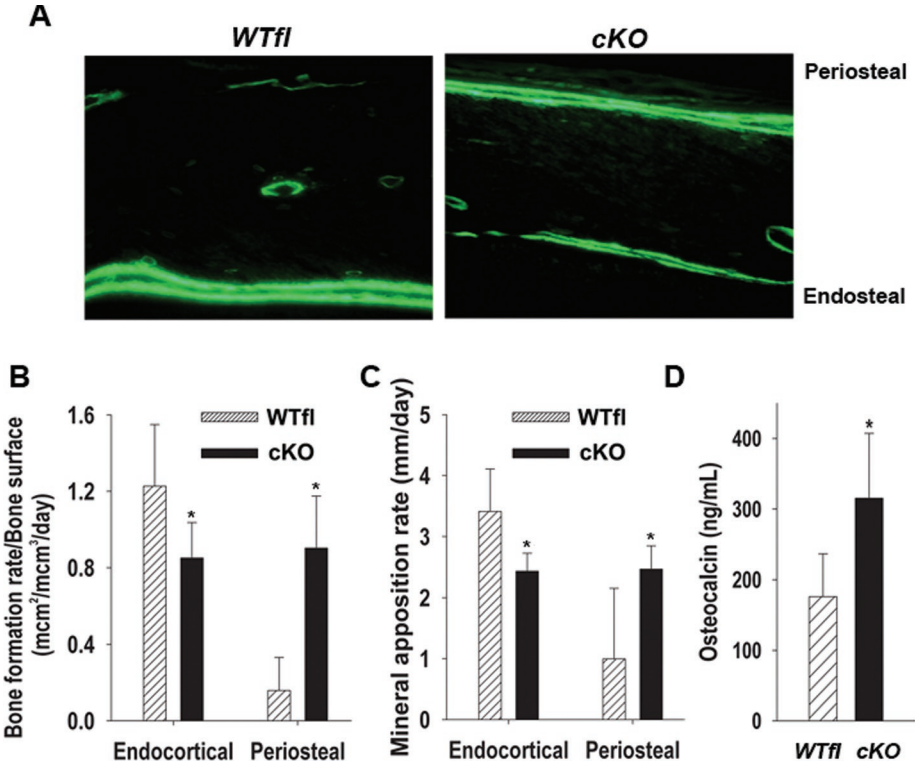

FIGURE 4: Altered cortical bone formation in cKO mice. (A) Fluorescence micrographs of calcein labels on the cortical surfaces of WTfl and cKO femurs at 1 mo of age. Double label is seen only on the endocortical surface of the WTfl bone, whereas abundant double label is seen on the periosteal surface and to a lesser extent on the endosteum of cKO bone. (B) Bone formation rate and (C) mineral apposition rate are decreased on the endosteal surface in cKO bones, whereas they are both significantly higher on the periosteal surface of mutant mice relative to WTfl controls (*, $P < 0.05$, *t*-test for unpaired samples, n = 4). (D) Serum osteocalcin levels, from 1-mo-old mice, are significantly increased in the cKO relative to WTfl (*, $P < 0.05$, *t*-test for unpaired samples, n = 7–8).

increased osteoclast number reflects an indirect effect of the mutant osteoblast. First we verified that bone marrow–derived macrophages (used as osteoclast precursors) from both WTfl and cKO mice produced similar numbers of osteoclasts when grown in the presence of M-CSF and RANKL (Figure 7, D and E). We also verified by Western blot analysis that *Gja1* ablation does not occur in the osteoclast lineage of cKO mice, as both cKO and WTfl macrophages and multinucleated TRAP+ cells express Cx43 (Figure 7F). Next we examined expression of osteopotegerin (*Opg*) and *Rankl*, two key osteoclast regulators produced by osteoblasts. Whereas expression of *Rankl* mRNA was unaltered in cKO mice, the abundance of *Opg* mRNA, an inhibitor of osteoclastogenesis, was significantly down-regulated in cKO relative to WTfl mice (Figure 7G). We then tested the osteoclastogenic potential of wild-type and mutant osteoblastic cells by coculturing bone marrow–derived stromal cells with macrophages isolated from either cKO or WTfl mice. When stromal cells derived from WTfl mice were used to support in vitro osteoclastogenesis, similar numbers of osteoclasts formed regardless of the osteoclast precursor genotype. However, when either cKO or WTfl macrophages were cocultured with cKO stromal cells, a fourfold higher number of multinucleated TRAP+ osteoclasts were obtained (Figure 7, H and I). Thus it is an abnormality in the stromal/osteoblast lineage that determines the increased osteoclastogenesis observed in Cx43-deficient mice.

DISCUSSION

These studies demonstrate that ablation of *Gja1* or replacement of one wild-type *Gja1* allele with a mutant linked to ODDD in chondro-osteoprogenitor cells causes a high bone turnover phenotype with increased periosteal bone formation, but abnormal osteoblast function and indirect endocortical osteoclast activation. This leads to age-dependent cortical bone expansion, cortical thinning, and deposition of abnormal bone tissue. Thus Cx43 controls both arms of bone remodeling via the osteoblast.

In previous work, we have ablated *Gja1* in committed osteoblasts and osteocytes and found that these mice are osteopenic and have functionally defective osteoblasts (Chung *et al.*, 2006), widened diaphysis of long bones, and decreased bone strength (Grimston *et al.*, 2008). Here, using the *DM1* promoter to obtain a broader and earlier *Gja1* ablation, we observe a similar but more severe phenotype, as well as developmental abnormalities, such as hypoplastic, hypomineralized skulls, smaller thoracic cavities, and shorter limbs. Such dyspmorphic features are similar to those observed in germline *Gja1* null mice (Lecanda *et al.*, 2000). At variance with our previous observations (Chung *et al.*, 2006), we found very low, if any, expression of *LacZ* in trabecular bone cells of cKO mice. The reasons for such discrepancy are unclear but could be related to either low *Gja1* expression in trabecular bone or lower efficiency of Cre activity on the *Gja1* allele than on the *ROSA26* reporter allele. Interestingly, in mice where *Gja1* was deleted using the *Bglap* promoter, the phenotype is also restricted to cortical bone (Plotkin *et al.*, 2008; Bivi *et al.*, 2009). Hence larger diaphyseal cross-sectional area and cortical thinning are the most consistent phenotypic changes present in adult *Gja1* cKO mice, now reported in three difference genetic models. Similar cortical abnormalities are seen in cODDD mice and were also evident in $Gja1^{Jrt/+}$ mice, a mutant with a phenotype closely resembling ODDD (Flenniken *et al.*, 2005), further proving that modeling of cortical architecture is the main function of Cx43 in adult bone.

Our studies show that this phenotype is the result of a complex mechanism involving both arms of the bone remodeling cycle. Cortical bone expansion is primarily due to accelerated endocortical bone resorption, leading to widening of the medullary cavity, which is only partially compensated for by an exuberant periosteal bone apposition resulting in a larger periosteal perimeter but thinner cortices. Earlier in vitro studies have postulated a role of Cx43 in osteoclast function (Ransjo *et al.*, 2003; Matemba *et al.*, 2006). However, our genetic modification excludes osteoclasts, and the coculture studies establish that the exuberant osteoclastogenesis is entirely dependent on Cx43-deficient osteoblast-supporting cells, which produce an abnormally low abundance of *Opg*, a key inhibitor of osteoclast differentiation. Further evidence that an abnormal OPG/RANKL balance is a key mechanism of the *Gja1* cKO phenotype is provided by the finding that addition of exogenous osteoclastogenic factors, M-CSF and RANKL, to the cocultures offsets the

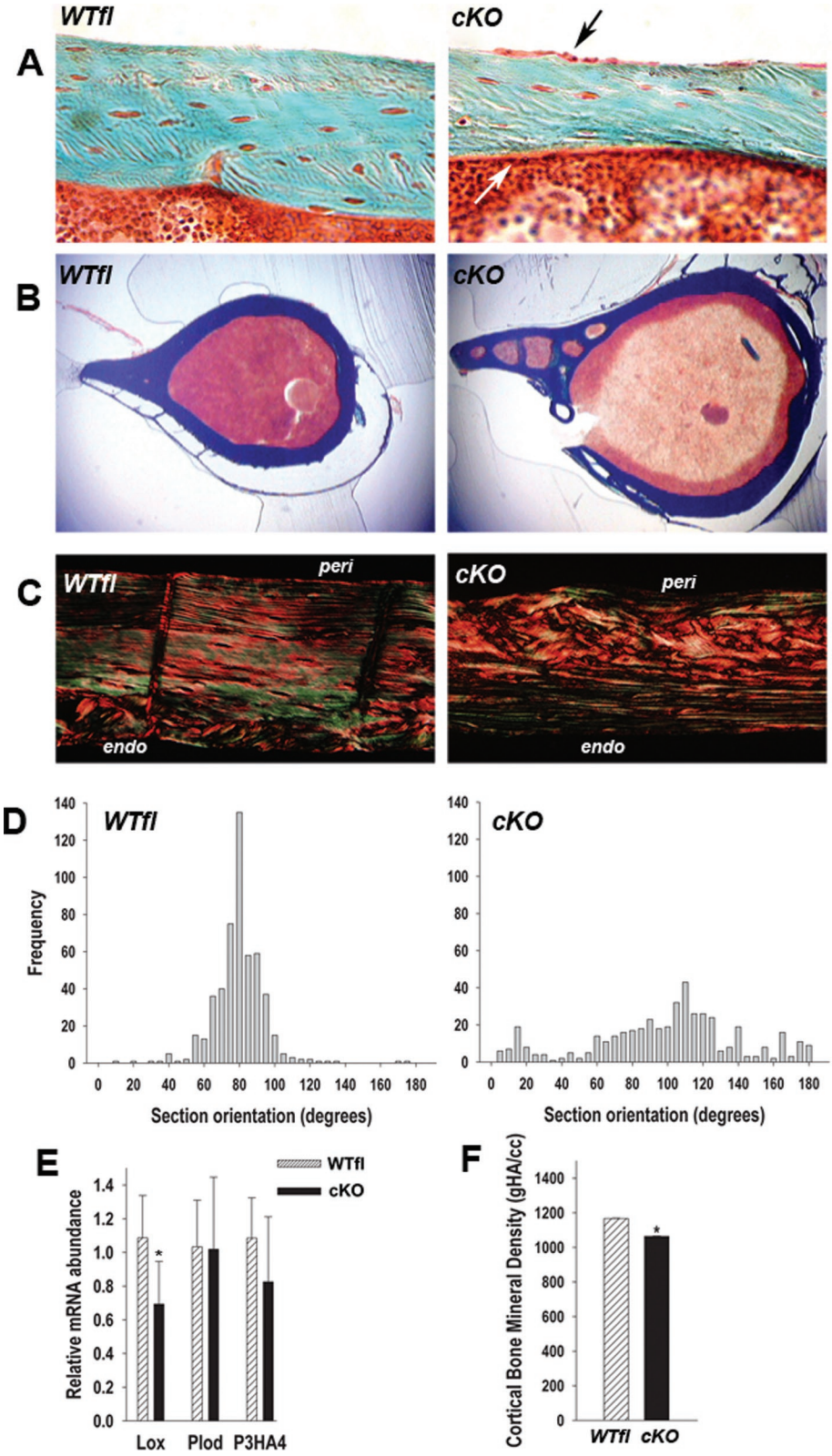

FIGURE 5: Abnormal cortical bone properties in cKO mice. (A) At 1 mo of age, Goldner trichrome stain show thinner cKO cortices relative to WTfl, but no abnormal osteoid. Also note the prominent osteoblast layer in the periosteum (black arrow) and endosteum (white arrow) in cKO sections. (B) Low-magnification Goldner trichrome-stained cross-sections showing increased cortical porosity and larger cross-sections in cKO bone relative to WTfl. (C) Birefringence of picrosirius red stained cortical sections show more collagen disorganization and a woven bone aspect in cKO relative to WTfl, especially on the periosteal side. (D) Collagen fiber orientation was quantitated by measuring the angle of extinction of polarized light in picrosirius red stained sections. Whereas collagen fiber orientation clusters around 90 degrees in the WTfl, there is a wide, uneven spread of collagen fiber orientation across the whole range (n = 4). (E) Quantitative real-time PCR of femoral bone (without bone marrow) RNA extracts, revealing lower abundance of *Lox* mRNA, but unchanged *Plod* and *P3HA4* mRNA in cKO relative to WTfl. (F) Cortical bone mineral density (gHA/cc) measured by μCT showing a significant reduction in the cKO relative to WTfl (*, $P < 0.05$ vs. WTfl, *t*-test for unpaired samples; n = 4–6).

difference in osteoclastogenesis between WTfl and cKO cells.

The increased periosteal bone apposition detected in cKO long bones contrasts with decreased endosteal bone formation, also present in *Gja1* ablated mice driven by the *Col1A1* promoter (Chung *et al.*, 2006; Grimston *et al.*, 2008), and accounts for the progressive diaphyseal cross-section expansion, perhaps representing a compensatory reaction to increased endosteal bone erosion. The mechanism leading to the endosteal-to-periosteal bone formation shift remains to be elucidated, though our data suggest a possible link to reduced expression of *Sost*, an inhibitor of Wnt signaling (Krishnan *et al.*, 2006). Notably, *Sost*-deficient mice exhibit cortical thickening and increased tissue area with increased periosteal and endosteal bone apposition (Li *et al.*, 2008; Lin *et al.*, 2009). Diaphyseal expansion in cKO mice is not present at birth but develops with age, and may reflect an impaired ability of Cx43-deficient animals to adapt to environmental factors. Cx43-deficient mice are less sensitive to anabolic mechanical load (Grimston *et al.*, 2008) and skeletal unloading (Grimston *et al.*, unpublished data); and Cx43 has been implicated in mechanotransduction, primarily in osteocytes (Cherian *et al.*, 2005; Genetos *et al.*, 2007). This loss of sensitivity to mechanical stimuli may be the fundamental mechanism by which Cx43 loss leads to age-dependent changes in cortical bone. Intriguingly, sclerostin-deficient mice are also insensitive to in vivo mechanical skeletal unloading (Lin *et al.*, 2009), reinforcing the hypothesis that Cx43 may regulate adaptive responses to mechanical stimuli via modulation of sclerostin production.

Not only is cortical bone thinner in the cKO, the quality of the bone tissue is also abnormal, with disorganized collagen fibers, increased porosity, and decreased mineralization. All these factors may explain the reduced bone strength and stiffness

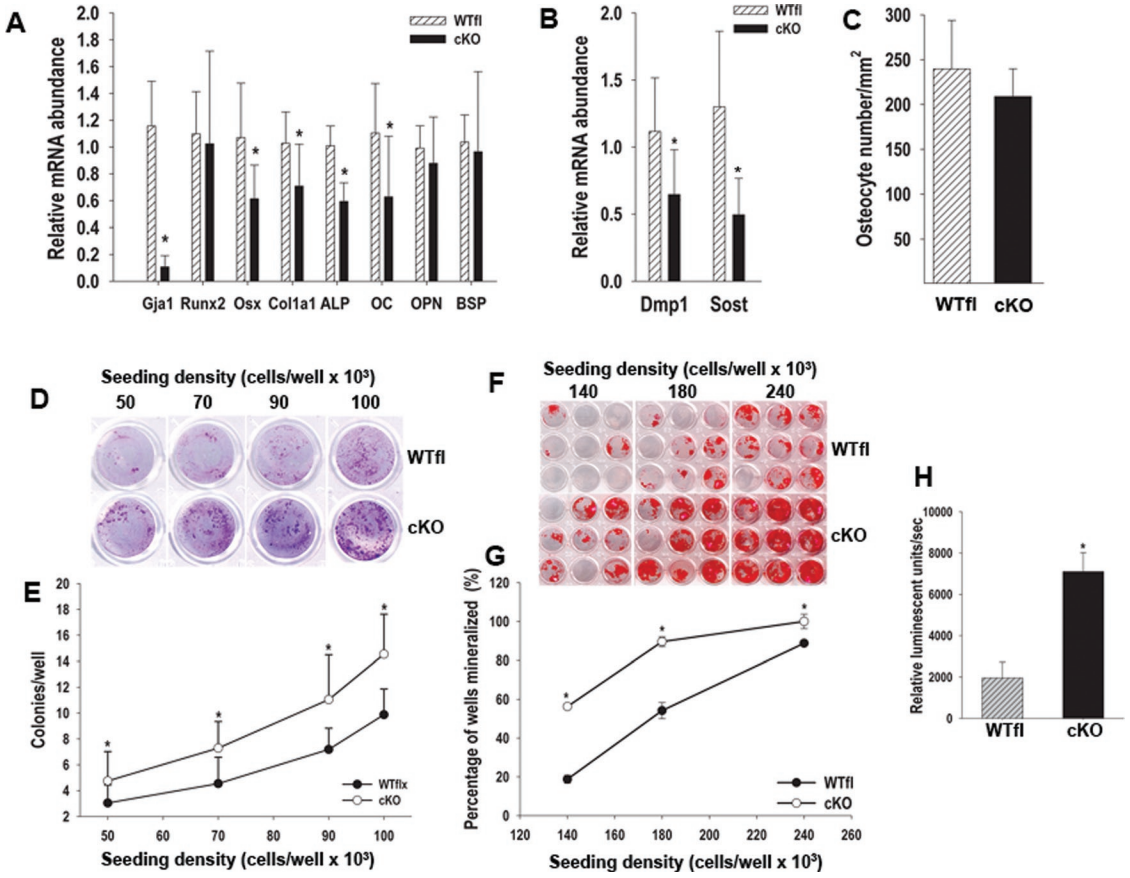

FIGURE 6: Abnormal osteoblast differentiation and function in cKO mice. (A) Quantitative real-time PCR on RNA extracts from 3-mo-old femurs after bone marrow removal. Data are normalized to *Cphn* and expressed as mRNA abundance relative to WTfl bones. Many, though not all osteoblast genes are down-regulated in cKO bones. (B) Quantitative real-time PCR on cortical bone reveals significantly lower *Dmp1* and *Sost* mRNA abundance in cKO bones. (C) The number of osteocyte per cortical area, assessed in Masson trichrome-stained, 1-mo-old sections is not different between WTfl and cKO femurs. (D) Unfractionated, adherent bone marrow cells were isolated, grown for 14 d at different seeding densities, and stained with Giemsa for CFU-F analysis, as detailed in *Materials and Methods*. (E) At each seeding density, there is a significantly higher CFU-F number (colonies with >50 cells) in cKO than in WTfl cultures. Each well represents 1 of 24 replicates at the corresponding seeding densities. (F) Bone marrow cells were similarly isolated, but cultured in mineralizing medium for 21 d, before alizarin red staining. (G) The percentage of wells that mineralized was used as an index of CFU-O, and this percentage is higher in cKO than in WTfl at each seeding density. Each group of nine wells is representative of each of the three seeding densities used. (H) Unfractionated, adherent bone marrow cells were assayed for BrdU incorporation over a 6-h period, using a chemiluminescent detection system. BrdU incorporation is about threefold higher in cKO than in WTfl cultures (*, $P < 0.05$, vs. WTfl; *t*-test for unpaired samples; n = 3 or 4).

despite the increased geometric moment of inertia of the larger cKO diaphyses. Whereas increased porosity underlies enhanced bone resorption, analysis of the material properties of cKO bones did not reveal major qualitative defects in either the mineral or organic phase. The emerging picture is that of a hypomineralized, woven, and immature bone, which might be the consequence of accelerated remodeling and inefficient matrix production response by Cx43-deficient osteoblasts. Alternatively, the accelerated periosteal bone formation (and endosteal bone resorption) might represent a mechanism to increase bone strength in response to this defective bone matrix in cKO mice. Regardless of whether the increased cortical turnover is the cause or a consequence of the abnormal material properties of cKO bones, a primary osteoblast defect is the cause of the entire phenotype.

Many osteoblast gene products are down-regulated in the cKO in addition to *Opg*, including *Osx*, *Bglap*, and *Alpl*, but not *Runx2*. Because *Gja1* is ablated early in the chondro-osteogenic lineage, before *Runx2* expression, these results indicate that Cx43 regulates progression of osteoblast differentiation at the *Runx2-Osx* transition, resulting in down-regulation of most downstream osteoblast genes consistent with previous findings (Lecanda *et al.*, 2000; Chung *et al.*, 2006). Interestingly, Cx43 enhances *Runx2* phosphorylation, DNA binding activity, and *Runx2*-mediated gene transcription (Lima *et al.*, 2009). Osteocyte-specific genes, *Dmp1* and *Sost*, are also down-regulated in the cKO and may be part of this osteoblastic defect. However, cKO bone marrow stromal cells (BMSCs) exhibit significantly higher proliferative capacity, likely resulting in the increased number of bone marrow uncommitted precursors and osteoprogenitors. Higher proliferative activity may also explain the increased number of periosteal cells and the increased periosteal bone formation rate.

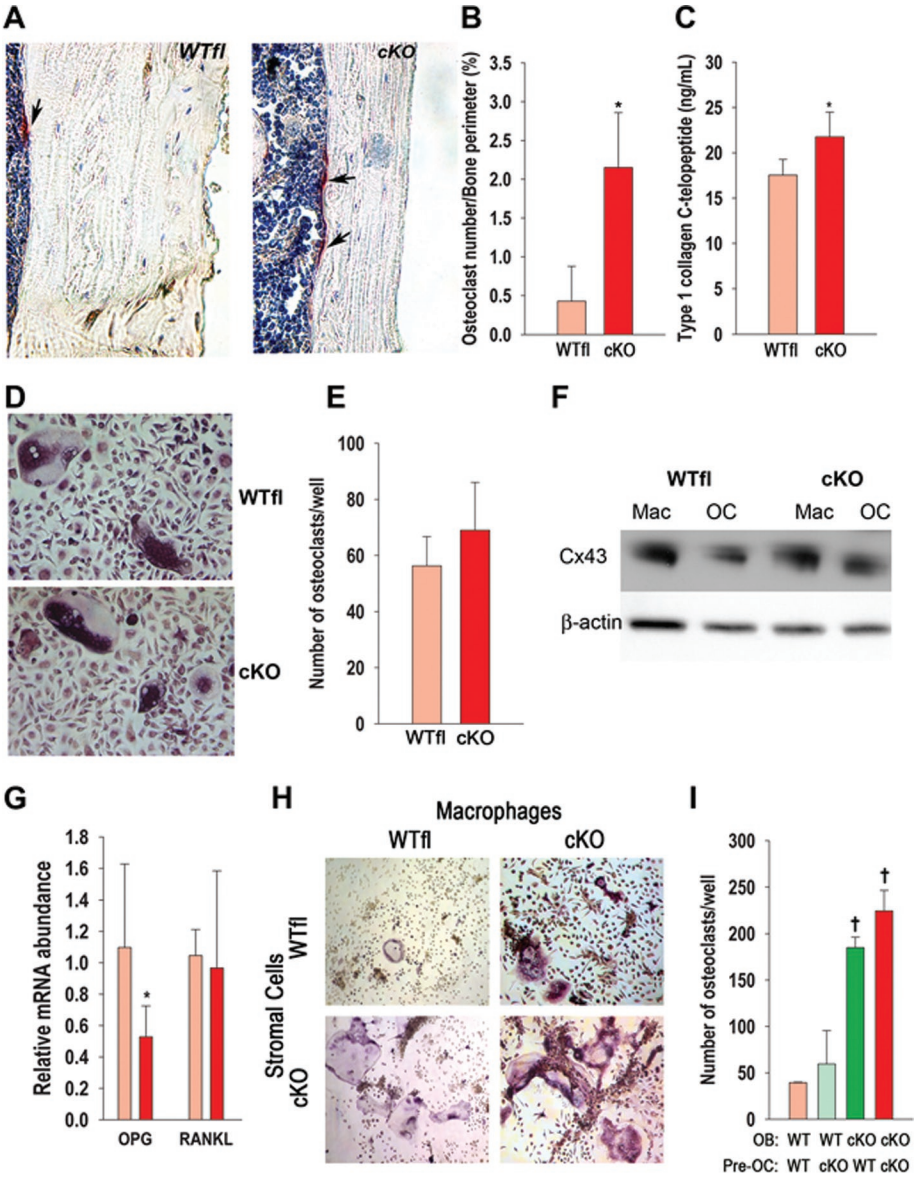

FIGURE 7: Increased osteoclastogenesis and bone resorption in cKO mice. (A) Sections of cortical bone from 1-mo-old mice showing endocortical TRAP+ cells of both WTfl and cKO bones (arrows). (B) The number of osteoclasts (multinucleated TRAP+ cells) on the endocortical surface is significantly higher in cKO than in WTfl. (C) Serum C-terminal telopeptides of type I collagen is also increased in cKO relative to WTfl. (D) Osteoclast precursors (macrophages) isolated from either cKO or WTfl bone marrow were cultured in 96-well plates for 5 d in the presence of M-CSF and RANKL. (E) No differences in the number of TRAP+, multinucleated osteoclasts were observed between genotypes. (F) Macrophages (Mac) isolated from either cKO or WTfl bone marrow and cultured for 5 d in the presence of M-CSF, and osteoclasts (OC), obtained by further incubation of macrophages with M-CSF and RANKL, were lysed for immunoblotting. Cx43 expression was lower in mature osteoclasts relative to macrophages in both genotypes with no difference between genotypes. (G) The abundance of *Opg* mRNA, assessed by real-time PCR in extracts from femurs (without bone marrow), is lower in cKO relative to WTfl, whereas *Rankl* mRNA is not different. (H) Osteoblasts and osteoclast precursors isolated from either cKO or WTfl bone marrow were cocultured in 24-well plates for 7 d in medium supplemented with vitamin D and dexamethasone, for development of TRAP+, multinucleated osteoclasts. (I) Osteoblasts from WTfl mice support the same number of osteoclastic cells regardless of the genotype of the osteoclast precursors, whereas when cKO osteoblasts are used, a higher number of osteoclast form regardless of the osteoclast precursor genotype (*, $P < 0.05$, vs. WTfl, *t*-test for unpaired samples, n = 5-8; †, $P < 0.05$ vs. WT OB; Tukey test; n = 4).

Introduction of the G138R *Gja1* mutation, linked to ODDD, in chondo-osteogenic cells recapitulates the most relevant skeletal features of cKO mutants. This phenotype is caused by replacement of a single wild-type allele, and because *Gja1* heterozygous null mice have a normal skeleton (Lecanda *et al.*, 2000; Chung *et al.*, 2006), the G138R *Gja1* mutant is indeed dominant-negative for Cx43, as postulated by in vitro studies (Roscoe *et al.*, 2005). Furthermore, as this mutant has also been shown to enhance hemichannel function (Gong *et al.*, 2007; Dobrowolski *et al.*, 2008), our results argue against the hypothesis that hemichannel activity is involved in bone turnover modulation. Severe whole-body osteopenia and larger but thinner femoral diaphyses were also observed in other ODDD mouse models (Flenniken *et al.*, 2005; Dobrowolski *et al.*, 2008). Intriguingly, osteopenia has never been described in patients with ODDD, who are typically reported as having hyperostosis of the cranial vault (Loddenkemper *et al.*, 2002; Paznekas *et al.*, 2003; Kjaer *et al.*, 2004). These discrepancies may reflect species-related differences, though bone mass measurements have never been reported in ODDD patients. However, broad tubular bones are frequently observed in ODDD patients, and this feature may indeed reflect the cortical bone expansion and attendant high bone remodeling emerging from this study.

In summary, Cx43 modulates both arms of the bone-remodeling cycle in adult bones via cell autonomous and noncell autonomous actions, causing indirect activation of endocortical osteoclasts and resulting in age-dependent cortical bone expansion and cortical thinning. This is not effectively compensated by increased periosteal bone formation, as the material properties of the newly formed bone are abnormal, resulting in compromised bone strength. Such changes are remindful of those that occur in aging and disuse osteoporosis.

MATERIAL AND METHODS

Transgenic mice

For conditional *Gja1* ablation, a mouse strain harboring a mutant "floxed" *Gja1* allele ($Gja1^{flox}$) (Theis *et al.*, 2001) was mated to mice expressing *Cre* under control of the *DM1* promoter (*DM1-Cre*) (Yu *et al.*, 2003), resulting in Cre-mediated replacement of the entire *Gja1* reading frame with the *LacZ* reporter cassette. To avoid potential effects of Cre activation in the parental germ line (Theis *et al.*, 2001), and following a previously described strategy (Chung *et al.*,

2006), we crossed *Gja1*$^{flox/flox}$ mice with *DM1-Cre* mice also carrying a *Gja1* null allele (*DM1-Cre;Gja1*$^{+/-}$). These crosses produce, in approximately equal numbers, *Gja1* conditionally deleted mice, *DM1-Cre;Gja1*$^{flox/-}$ (cKO), as well as *Gja1*$^{flox/+}$ (wild-type equivalent; WTfl), *Gja1*$^{flox/-}$ (heterozygous equivalent), and *DM1-Cre;Gja1*$^{flox/+}$ (conditional heterozygous). Since we found that the latter two genotype groups have no detectable phenotypic abnormalities, only data from cKO and WTfl are reported here.

To induce an ODDD mutation selectively in chondro-osteoprogenitor cells, we mated *DM1-Cre* with *Gja1*$^{flox(G138R)/flox(G138R)}$ mice, a kind gift from Klaus Willecke (University of Bonn, Germany). Analogously to the "floxed" *Gja1* mutant, Cre-mediated recombination in the *Gja1*$^{flox(G138R)}$ mice removes the wild-type *Gja1* allele, replacing it with a *Gja1* G138R mutant allele (Dobrowolski *et al.*, 2008). These crosses generate conditional heterozygous mutants, *DM1-Cre;Gja1*$^{flox(G138R)/+}$ (cODDD), and wild-type equivalent *Gja1*$^{flox(G138R)/+}$ (WTod) mice. Because of the gender-specific differences in bone structure, male and female mice were analyzed separately, but we present data on male mice as similar results were obtained in both genders. ROSA26 mice (a generous gift from Henry Kronenberg, Harvard University, Boston, MA) were mated with *DM1-Cre* mice to determine the effectiveness of *DM1*-driven Cre recombination in adult mice (Soriano, 1999).

Genotyping was performed by PCR on genomic DNA extracted from mouse tails using the HotSHOT method (Truett *et al.*, 2000). We used previously described methods to detect the *Gja1* null, wild-type, floxed alleles (Chung *et al.*, 2006) and *Gja1*$^{flox(G138R)}$ alleles (Dobrowolski *et al.*, 2008), as well as the *DM1-Cre* (Liu *et al.*, 2002) and ROSA26 transgenes (Mao *et al.*, 1999).

All the mouse lines used in this project were developed in a mixed C57BL/6-C129/J background, and littermates were used as controls. Mice were fed regular chow ad libitum and housed in a room maintained at constant temperature (25°C) on a 12-h light and 12-h dark schedule. All procedures were approved by the Animal Studies Committee of Washington University in St. Louis.

Whole body mounts

Newborn mice were stained with alizarin red and alcian blue as previously described (Chung *et al.*, 2006).

Bone mass and microstructure

Whole-body bone mineral content and BMD were monitored by DXA using a PIXImus scanner (GE/Lunar, Madison, WI) under anesthesia as previously described (Castro *et al.*, 2004). Analysis of femoral bone structure was performed using a μCT system (μCT 40; Scanco Medical AG, Zurich, Switzerland), as also previously described (Grimston *et al.*, 2008; Di Benedetto *et al.*, 2010). μCT of skulls from 1-mo-old mice were also performed. Skulls were stabilized in 1.5–2.0% agarose gel and scanned using 45 EkVp radiation energy at standard resolution (20 μm). About 250 images were used for 3D reconstruction.

Bone biomechanics

Mechanical testing in a three-point bending to failure was conducted on femora after μCT scanning as described previously (Di Benedetto *et al.*, 2010).

Bone histology and histomorphometry

Mice were labeled twice by injection of calcein (15 mg/kg i.p.; Sigma-Aldrich, St. Louis, MO) 7 and 2 d before euthanasia, which was performed under light anesthesia by exsanguination through dorsal aortic puncture. Blood was collected and the serum stored at −80°C for later assays. Bone samples were prepared as previously described with some modifications (Chung *et al.*, 2006). Quantitative histomorphometry was performed as detailed elsewhere (Castro *et al.*, 2004; Grimston *et al.*, 2006). Some undecalcified sections were stained with a Goldner's modified trichrome technique, which was also used on thick (80 μm) sections to visualize cortical porosity (Hirano *et al.*, 2000).

Some decalcified bone samples were processed for β-gal staining as detailed (Chung *et al.*, 2006), with the addition of 100 mM galactose to the staining solution to quench nonspecific staining. To study collagen fiber orientation, paraffin sections were stained in 0.1% picrosirius red solution, destained in 1% (v/v) acetic acid, and counterstained with hematoxylin. The samples were visualized on a polarized light microscope (Olympus BX51P; Olympus, Tokyo, Japan), and images were analyzed as previously described (Thomopoulos *et al.*, 2006).

Bone marrow stromal progenitor cells

We used a modification of a previously described method (Castro *et al.*, 2004; Di Benedetto *et al.*, 2010). The entire marrow cavity of the shafts (femora and tibiae) of 3-mo-old mice was flushed by removing one of the epiphyses and centrifuging the bone at 10,000 rpm for 15 s. After hemolysis in a red blood cell lysis buffer (Roche Applied Science, Mannheim, Germany), the material was resuspended in αMEM (Mediatech, Herndon, VA) and filtered through a 70-μm cell strainer. Cells were resuspended in αMEM containing 20% fetal calf serum (FCS) and antibiotics and plated in 96-well tissue culture plates at different seeding densities for determination of colony forming unit-fibroblast (CFU-F) or -osteoblast (CFU-O). For CFU-F, cells were seeded in αMEM supplemented with 20% FCS. The number of CFU-F was determined after 14 d of culture by fixation in ethanol and staining with Giemsa. Colonies containing more than 50 cells were counted. For CFU-O assessment, cells were seeded in α-MEM supplemented with 20% FCS, 50 μM ascorbic acid, and 10 μM β-glycerophosphate. Cells were cultured for 21 d, then fixed in 50% ethanol/18% formaldehyde, and stained for mineralized matrix using alizarin red. Wells that stained were counted positive for mineralization, and the percentage of the 24 replicate wells in each plate that mineralized was calculated for all cell densities. All CFU experiments were undertaken in triplicate.

Osteoclast cultures

The marrow cavity was flushed as described above. Cells were resuspended in αMEM (Mediatech, Manassas, VA) and filtered through a 70-μm cell strainer. Cell were resuspended in αMEM containing 10% FCS, antibiotics, and 100 ng/ml M-CSF and cultured for 5 d, with media being replenished every second day. Thereafter, resultant macrophages were released and 3.0×10^5 cells seeded in a 96-well plate in α-MEM supplemented with 10% fetal bovine serum (FBS), 10 ng/ml M-CSF, and 100 ng/ml RANKL. Cells were grown for 7 d and then stained for TRAP using the Leukocyte Acid Phosphatase kit (Sigma-Aldrich, St. Louis, MO). The number of multinucleated, TRAP+ cells was determined as index of osteoclastogenesis.

Stromal cell-macrophage cocultures

BMSCs were isolated as described above, resuspended, and cultured in α-MEM supplemented with 10% FCS for 24 h. Nonadherent cells, which include macrophages, were removed and replated in a separate Petri dish in α-MEM supplemented with 10% FCS that favors macrophage growth. Adherent cells were cultured for 7 d in α-MEM supplemented with 20% FCS to stimulate proliferation of

BMSCs. Thereafter, stromal cells and macrophages were released from their respective dishes, mixed (3.4×10^5 each), and seeded in a 24-well plate in α-MEM supplemented with 10% FBS, 10 nM vitamin D3, and 100 nM dexamethasone (Wang *et al.*, 2004). These cocultures were incubated for 7 d and then stained for TRAP as described above.

Cell proliferation

BMSCs were isolated as described above, counted, and seeded in α-MEM supplemented with 20% FBS on a black-sided, 96-well tissue culture plate. Twenty-four hours later, the cells were labeled with BrdU, and incorporation was quantified using a chemiluminescent Cell Proliferation ELISA kit as per manufacturer's instructions (Roche Applied Science, Mannheim, Germany).

Real-time quantitative PCR

Total RNA was extracted from whole bones that had been flushed of bone marrow as described above and flash frozen in liquid nitrogen. Bones were pulverized using a Braun Mikrodismembrator (Sartorius Stedim Biotech S.A., Aubagne, France). Total RNA was extracted using TRIzol reagent (Invitrogen, Carlsbad, CA) and further purified using Phase-Lock gel tubes (5 Prime, Hamburg, Germany) and Qiagen RNA Easy kit (Qiagen, Valencia, CA) as per the manufacturer's instructions. Contaminating DNA was removed by RNase-free DNase (Qiagen, Valencia, CA) treatment. mRNA was quantified following previously described methods (Stains *et al.*, 2003; Mbalaviele *et al.*, 2005), and 1 μg total RNA was reverse transcribed using a Superscript VILO cDNA synthesis kit (Invitrogen, Carlsbad, CA). Real-time PCR analysis performed in an Applied Biosytem 7500 Fast detector system using the SYBR green PCR method according to manufacturer's instruction (Applied Biosystems, Foster City, CA). The mean cycle threshold value (Ct) from triplicate samples was used to calculate gene expression, and PCR products were normalized to *Cphn* levels for each reaction. Relative gene expression levels were determined as described in User's Bulletin (P/N 4303859) from Applied Biosystems. Primer sets are detailed in Supplemental Table 1. Taqman Gene expression assays (Applied Biosystems) were used for quantification of *Dmp1*, *Lox*, *Plod,* and *P3ha4*, according to manufacturer's instruction (Applied Biosystems).

Biochemical markers of bone turnover

Serum C terminus Cross-Linked Telopeptides of Type I Collagen (CTX) and osteocalcin were measured as indices of bone resorption and formation, respectively. For these assays, serum was obtained from mice that had been deprived of food and water for 6 h. Analyses were performed by ELISA, using a CTX (RatLaps EIA; Immunodiagnostics Systems, Fountain Hills, AZ) and the osteocalcin kit (Mouse Osteocalcin EIA Kit; Biomedical Technologies, Stoughton, MA), according to the manufacturer's instructions.

Immunoblotting

Protein extracts were prepared from whole bones that had been flushed of bone marrow and processed as described earlier. The pulverized bone was incubated in 50 mM Tris, pH 8.0, 150 mM NaCl, 2 mM EDTA, 1% Triton-X, 0.1% SDS, 0.5% sodium deoxycholate, 2 mM $NaVO_4$, 10 mM NaF, and protease inhibitors at 4°C for 10 min then centrifuged at 12,000 *g* for 20 min. Total protein concentration was measured using the BCA method (Pierce, Rockford, IL) and normalized against extraction buffer. Protein from osteoclast cultures was isolated using the same method, after removal of adherent stromal cells from six-well cultures by incubation with 10 mM EDTA for 5 min at 37°C. Proteins were separated on 8% Tris-glycine SDS gel and transferred to Immobilon membranes (Millipore, Billerica, MA). The membrane was probed with antibodies against Cx43 (C6219; Sigma-Aldrich), β-gal (ab616; Abcam, Cambridge, MA), and α-tubulin (sc-8035; Santa Cruz Biotechnology, Santa Cruz, CA).

FTIR analysis

Femur midshafts from WTflx and cKO animals were collected, soft tissues removed, and the bone marrow removed by centrifugation and the samples lyophilized. The samples were pulverized and studied in transmission mode in KBr pellets using Bucker Vertex 70 FTIR spectrometer (Millipore, Billerica, MA). The spectra were collected with the resolution of 2 cm^{-1} with 32 scans collected per each spectrum.

Statistical analysis

Groups means were compared by *t*-test for unpaired samples. Data on repeated measures were analyzed by analysis of variance (ANOVA). Data were analysed using SigmaPlot Vs11.0 (Systat Software GmbH, Germany). All data are expressed as the mean ± SD.

ACKNOWLEDGMENTS

Part of this work has been presented at the 31st annual meeting of the American Society for Bone and Mineral Research, Denver, CO, September 2009. This work was supported by NIH Grants R01 AR041255, AR055913, and AR056678 (to R.C.). The authors thank Roberta Faccio and Viviana Cremasco, Department of Orthopaedic Surgery, Washington University, for their help with the osteoclastogenesis assay; Christine Donsante, Devang Sanghavi, Emily Nuse, Joanna Urbanski, and Laura Banks for technical assistance; and the Research Center for Auditory and Vestibular Studies Histology Core, Washington University (supported by P30 DC004665).

REFERENCES

Bivi N, Aguirre JI, Vyas K, Allen M, Bellido T, Plotkin L (2009). Increased osteocyte apoptosis and bone resorption, and decreased strength of cortical but not trabecular bone in mice lacking connexin43 in osteoblasts and osteocytes. J Bone Miner Res 24 (Suppl 1), Available at http://www.asbmr.org/Meetings/AnnualMeeting/AbstractDetail.aspx?aid=77a3ec41-fa04–4fec-95f2-a032eea3e807.

Castro CH, Shin CS, Stains JP, Cheng SL, Sheikh S, Mbalaviele G, Szejnfeld VL, Civitelli R (2004). Targeted expression of a dominant-negative N-cadherin in vivo delays peak bone mass and increases adipogenesis. J Cell Sci 117, 2853–2864.

Cherian PP, Siller-Jackson AJ, Gu S, Wang X, Bonewald LF, Sprague E, Jiang JX (2005). Mechanical strain opens connexin 43 hemichannels in osteocytes: a novel mechanism for the release of prostaglandin. Mol Biol Cell 16, 3100–3106.

Chung DJ, Castro CH, Watkins M, Stains JP, Chung MY, Szejnfeld VL, Willecke K, Theis M, Civitelli R (2006). Low peak bone mass and attenuated anabolic response to parathyroid hormone in mice with an osteoblast-specific deletion of connexin43. J Cell Sci 119, 4187–4198.

Civitelli R, Stains JP, Shin CS, Jørgensen N (2008). Intercellular junctions and cell-cell communication in the skeletal system. In: Principles of Bone Biology, Vol. 1, eds. JP Bilezikian, LG Raisz, and TJ Martin, San Diego, CA: Academic Press, 425–444.

Di Benedetto A, Watkins M, Grimston S, Salazar V, Donsante C, Mbalaviele G, Radice GL, Civitelli R (2010). N-cadherin and cadherin 11 modulate postnatal bone growth and osteoblast differentiation by distinct mechanisms. J Cell Sci 123, 2640–2648.

Dobrowolski R *et al.* (2008). The conditional connexin43G138R mouse mutant represents a new model of hereditary oculodentodigital dysplasia in humans. Hum Mol Genet 17, 539–554.

Doty SB (1981). Morphological evidence of gap junctions between bone cells. Calcif Tissue Int 33, 509–511.

Flenniken AM *et al.* (2005). A Gja1 missense mutation in a mouse model of oculodentodigital dysplasia. Development 132, 4375–4386.

Genetos DC, Kephart CJ, Zhang Y, Yellowley CE, Donahue HJ (2007). Oscillating fluid flow activation of gap junction hemichannels induces ATP release from MLO-Y4 osteocytes. J Cell Physiol 212, 207–214.
Gong XQ, Shao Q, Langlois S, Bai D, Laird DW (2007). Differential potency of dominant negative connexin43 mutants in oculodentodigital dysplasia. J Biol Chem 282, 19190–19202.
Goodenough DA, Goliger JA, Paul DL (1996). Connexins, connexons, and intercellular communication. Annu Rev Biochem 65, 475–502.
Goodenough DA, Paul DL (2003). Beyond the gap: functions of unpaired connexon channels. Nat Rev Mol Cell Biol 4, 285–294.
Grimston SK, Brodt MD, Silva MJ, Civitelli R (2008). Attenuated response to in vivo mechanical loading in mice with conditional osteoblast ablation of the connexin43 gene (Gja1). J Bone Miner Res 23, 879–886.
Grimston SK, Screen J, Haskell JH, Chung DJ, Brodt MD, Silva MJ, Civitelli R (2006). Role of connexin43 in osteoblast response to physical load. Ann NY Acad Sci 1068, 214–224.
Hirano T, Burr DB, Cain RL, Hock JM (2000). Changes in geometry and cortical porosity in adult, ovary-intact rabbits after 5 mo treatment with LY333334 (hPTH 1–34). Calcif Tissue Int 66, 456–460.
Kjaer KW, Hansen L, Eiberg H, Leicht P, Opitz JM, Tommerup N (2004). Novel Connexin 43 (GJA1) mutation causes oculo-dento-digital dysplasia with curly hair. Am J Med Genet 127A, 152–157.
Krishnan V, Bryant HU, MacDougald OA (2006). Regulation of bone mass by Wnt signaling. J Clin Invest 116, 1202–1209.
Lecanda F, Warlow PM, Sheikh S, Furlan F, Steinberg TH, Civitelli R (2000). Connexin43 deficiency causes delayed ossification, craniofacial abnormalities, and osteoblast dysfunction. J Cell Biol 151, 931–944.
Li L, Cserjesi P, Olson EN (1995). Dermo-1: a novel twist-related bHLH protein expressed in the developing dermis. Dev Biol 172, 280–292.
Li X *et al.* (2008). Targeted deletion of the sclerostin gene in mice results in increased bone formation and bone strength. J Bone Miner Res 23, 860–869.
Lima F, Niger C, Hebert C, Stains JP (2009). Connexin43 potentiates osteoblast responsiveness to fibroblast growth factor 2 via a protein kinase C-delta/Runx2-dependent mechanism. Mol Biol Cell 20, 2697–2708.
Lin C, Jiang X, Dai Z, Guo X, Weng T, Wang J, Li Y, Feng G, Gao X, He L (2009). Sclerostin mediates bone response to mechanical unloading through antagonizing Wnt/beta-catenin signaling. J Bone Miner Res 24, 1651–1661.
Liu Z, Xu J, Colvin JS, Ornitz DM (2002). Coordination of chondrogenesis and osteogenesis by fibroblast growth factor 18. Genes Dev 16, 859–869.
Loddenkemper T, Grote K, Evers S, Oelerich M, Stogbauer F (2002). Neurological manifestations of the oculodentodigital dysplasia syndrome. J Neurol 249, 584–595.
Mao X, Fujiwara Y, Orkin SH (1999). Improved reporter strain for monitoring Cre recombinase-mediated DNA excisions in mice. Proc Natl Acad Sci USA 96, 5037–5042.
Matemba SF, Lie A, Ransjo M (2006). Regulation of osteoclastogenesis by gap junction communication. J Cell Biochem 99, 528–537.
Mbalaviele G, Sheikh S, Stains JP, Salazar VS, Cheng SL, Chen D, Civitelli R (2005). β-catenin and BMP-2 synergize to promote osteoblast differentiation and new bone formation. J Cell Biochem 94, 403–418.
McLachlan E, Plante I, Shao Q, Tong D, Kidder GM, Bernier SM, Laird DW (2008). ODDD-linked Cx43 mutants reduce endogenous Cx43 expression and function in osteoblasts and inhibit late stage differentiation. J Bone Miner Res 23, 928–938.
Palumbo C, Palazzini S, Marotti G (1990). Morphological study of intercellular junctions during osteocyte differentiation. Bone 11, 401–406.
Paznekas WA *et al.* (2003). Connexin 43 (GJA1) mutations cause the pleiotropic phenotype of oculodentodigital dysplasia. Am J Hum Genet 72, 408–418.
Plotkin LI, Lezcano V, Thostenson J, Weinstein RS, Manolagas SC, Bellido T (2008). Connexin 43 is required for the anti-apoptotic effect of bisphosphonates on osteocytes and osteoblasts in vivo. J Bone Miner Res 23, 1712–1721.
Ransjo M, Sahli J, Lie A (2003). Expression of connexin 43 mRNA in microisolated murine osteoclasts and regulation of bone resorption in vitro by gap junction inhibitors. Biochem Biophys Res Commun 303, 1179–1185.
Roscoe W, Veitch GI, Gong XQ, Pellegrino E, Bai D, McLachlan E, Shao Q, Kidder GM, Laird DW (2005). Oculodentodigital dysplasia-causing connexin43 mutants are nonfunctional and exhibit dominant effects on wild-type connexin43. J Biol Chem 280, 11458–11466.
Soriano P (1999). Generalized lacZ expression with the ROSA26 Cre reporter strain. Nat Genet 21, 70–71.
Stains JP, Civitelli R (2005). Gap junctions in skeletal development and function. Biochim Biophys Acta 1719, 69–81.
Stains JP, Lecanda F, Screen J, Towler DA, Civitelli R (2003). Gap junctional communication modulates gene transcription by altering the recruitment of Sp1 and Sp3 to connexin-response elements in osteoblast promoters. J Biol Chem 278, 24377–24387.
Theis M, de Wit C, Schlaeger TM, Eckardt D, Kruger O, Doring B, Risau W, Deutsch U, Pohl U, Willecke K (2001). Endothelium-specific replacement of the connexin43 coding region by a lacZ reporter gene. Genesis 29, 1–13.
Thomopoulos S, Marquez JP, Weinberger B, Birman V, Genin GM (2006). Collagen fiber orientation at the tendon to bone insertion and its influence on stress concentrations. J Biomech 39, 1842–1851.
Truett GE, Heeger P, Mynatt RL, Truett AA, Walker JA, Warman ML (2000). Preparation of PCR-quality mouse genomic DNA with hot sodium hydroxide and tris (HotSHOT). Biotechniques 29, 52, 54.
Wang MW, Wei S, Faccio R, Takeshita S, Tebas P, Powderly WG, Teitelbaum SL, Ross FP (2004). The HIV protease inhibitor ritonavir blocks osteoclastogenesis and function by impairing RANKL-induced signaling. J Clin Invest 114, 206–213.
Yu K, Xu J, Liu Z, Sosic D, Shao J, Olson EN, Towler DA, Ornitz DM (2003). Conditional inactivation of FGF receptor 2 reveals an essential role for FGF signaling in the regulation of osteoblast function and bone growth. Development 130, 3063–3074.